Efficiency improvement in photovoltaic solar cells by giant optical amplification: metallic Vs multi-dielectric coupling

Abdoulaye Sène, Césaire Ngor Ndiaye , Lamine Thiaw

Ecole Supérieure Polytechnique de Dakar, Université Cheikh Anta Diop de Dakar, SENEGAL

abdoulaye37.sene@ucad.edu.sn

cesairengor.ndiaye@esp.sn

lamine.thiaw@ucad.edu.sn

***Summary*— Today, photovoltaic energy is a strong alternative to meet part of the energy needs of today's society in order to reduce global warming due to the emission of greenhouse gases by fossil fuels. Thus, for several years, the photovoltaic industry has not stopped looking for solutions to increase the performance/cost ratio of photovoltaic solar cells. Many results and progresses have been achieved but the efficiency of current solar cells is still below expectations. The major challenge is to be able to absorb a large part of the light spectrum, which is why today's research is turning to a new technology, that of nanotechnologies, as well as the use of materials capable of having a better absorption coefficient of the light spectrum. In this context, Indium Gallium Nitride (InGaN) is one of the best candidates for the realization of a high efficiency thin film solar cell. To increase the light absorption and thus the efficiency of a cell, the light trapping plays a particularly important role. Thus, in this work, a synthesis method based on complex admittances widely used to synthesize optical functions was implemented in our previous work. The results of this work have shown that an optimal choice of the thickness of the optical thin films, the incidence and the wavelength of the illumination allows to obtain a total absorption and thus an exaltation of the optical field (10-10^4) in a metal or in a multi-dielectric structure. From these nanostructures exalting the optical field, it was possible to realize the coupling between these nanostructures and a solar cell based on Gallium-Indium Nitride (InGaN) in order to hope for record yields within the cell.**

***Keywords*— Photovoltaic energy, Solar cells, Exaltation, thin films, coupling, nanostructure**

I. INTRODUCTION

Solar photovoltaic (PV) energy can be defined as clean energy, because it comes from a source of energy that is non-polluting and inexhaustible on a human scale. It is obtained by the direct conversion of light into electricity using photovoltaic cells. This conversion is based on a physical phenomenon known as the photovoltaic effect, discovered by Alexandre Edmond Becquerel in 1839 [1], [2]. Today, the photovoltaic system plays an important role in the production of electrical energy, with the aim of reducing greenhouse gas emissions from fossil fuels [3], [4].

This proves that it is necessary to find technologies that will optimize its performance, which is still below expectations.

As a result, a great deal of research is turning to alternative thin-film materials (nitrides) to achieve higher yields at relatively low cost. Among the new thin-film materials being considered for photovoltaics, the InGaN alloy is one of the most widely used today. It has been studied for high-efficiency photovoltaic applications, thanks to its wide and adjustable energy gap, ranging from 0.7 eV to 3.42 eV [5].

In this context, a synthesis method for achieving arbitrary exaltations in metallic or multi-dielectric resonant nanostructured stacks has been developed in our previous work [6].

In this article, we first describe these multi-dielectric and metallic stacks and give the preliminary results obtained. Next, we describe the coupling of these resonant stacks with the solar cell, describing the configurations used and giving the final coupling results, which will enable us to evaluate the efficiencies obtained from these two configurations.

ISSN: 2356-5608

II. MULTI-DIELECTRIC VS. METAL STACKING

In this part, we are mainly interested in the nature of the material used as well as the design for the simulation of the absorption and the field strength using Matlab/Simulink software.

A. Description of the metal stack

The stacking structure used is of the form:

Glass/Gold/Air

This structure is formed by a superstrate (glass), a thin metallic layer of gold of 50 nm thickness and a substrate (air). The centering wavelength is 633 nm. The index of the superstrate (glass) is n0=1.52, that of the substrate (air) is ns=1 and for gold, it is 0.2 with an imaginary index of 3.2.

B. Description of the multi-dielectric stack

In this part, the stacking used for this structure is of the type:

Glass/$(HB)_2$ H/Air

This structure consists of a superstrate (glass), an alternation of 4 thin dielectric layers of High and Low index and the substrate (air).

The materials used are Tantalum Pentaoxide (Ta_2O_5) with index n_H=2.141 and silicon dioxide (SiO_2) with index n_B=1.457 and the centering wavelength is λ_c = 532 nm. The index of the superstrate (glass) is n_0=1.52 and that of the substrate (air) is n_s=1. The value of the imaginary index is 10^{-1}.

C. Preliminary results

In this part, we are mainly interested in the mapping of absorption and field intensity using Matlab/Simulink software.

1) Results obtained with the metal stack: The mapping of the absorption evolution as a function of wavelength and illumination angle corresponding to this stacking is calculated and presented in Fig. 1.

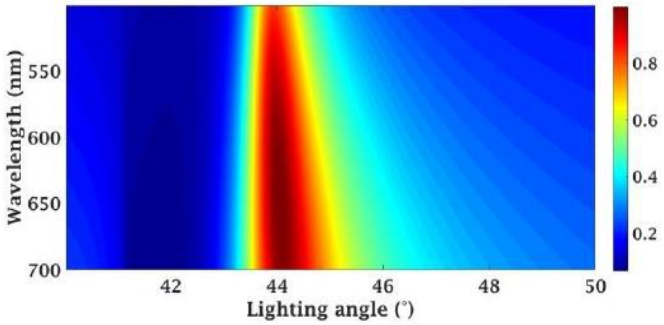

Fig. 1 Mapping of absorption as a function of wavelength and angle of incidence in TM mode with the metal structure

In this figure, we see that the absorption is total for several wavelengths for a particular incidence. In other words, all the energy is absorbed at the metal/dielectric interface when the resonance conditions are met.

This structure has a very wide absorption band due to the fact that the imaginary index of gold is high (3.2) compared to that of a dielectric. Indeed, the higher the imaginary index of the material, the wider the spectral or angular range of the resonance.

Note also that this total absorption is often accompanied by an exaltation of the electric field. By representing the evolution of the latter in the stack when the conditions of total absorption are met, we obtain the following Fig. 2.

ISSN: 2356-5608

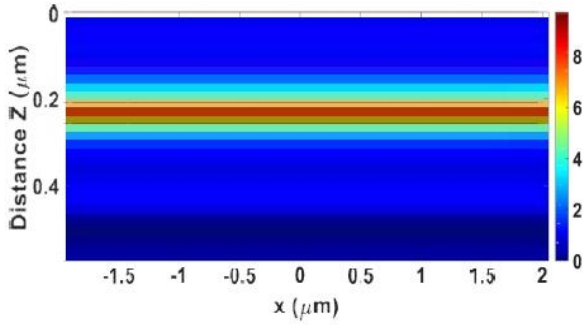

Fig. 2 Mapping of the electric field as a function of Z and X in TM mode when the metal structure is illuminated at the resonant frequency.

In this figure, the exaltation is maximum in the metal layer. This over-intensification reaches a rather modest value of 9.7 in the gold layer and this is due to the bandwidth of the resonance which is very wide. Indeed, the wider the resonance the less the exaltation.

2) Results obtained with the multi-dielectric stack: The mapping of the absorption evolution as a function of wavelength and illumination angle corresponding to this structure is calculated and presented in Fig. 3.

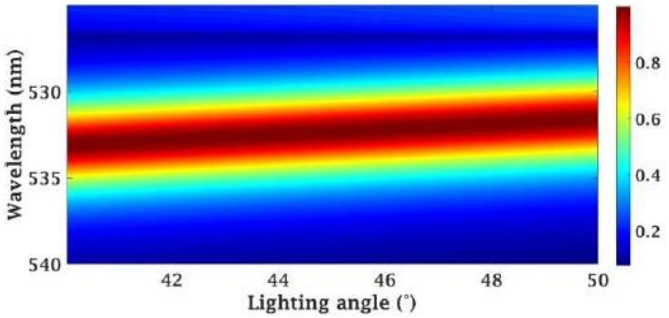

Fig. 3 Mapping of absorption as a function of wavelength and angle of incidence in TE mode with the multi-dielectric structure. The materials used are Ta_2O_5 and SiO_2

Here, the structure has a resonance with a much finer spectral width than that of the metallic structure thanks to its low imaginary index (0.1).

Representing the evolution of the associated electric field when the conditions of total absorption are met, we obtain Fig. 4 below.

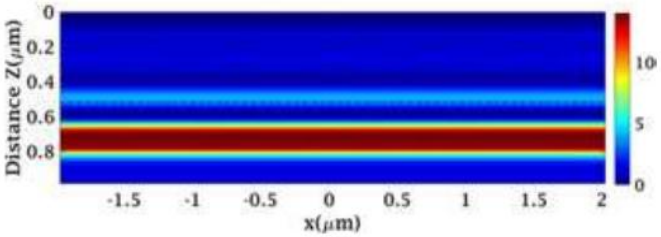

Fig. 4 Mapping of the electric field as a function of Z and X in TE mode when the multi-dielectric structure is illuminated at the resonance frequency

In this figure, the field is maximal in the last layer of the multi dielectric stack. This multi-dielectric structure using Tantalum Pentaoxide (Ta2O5) and Silicon Dioxide (SiO2) as materials is much cheaper compared to the metallic structure and gives a higher over-intensity of the order of 14. This high value is a consequence of the fineness of the resonance. Indeed, the narrower the resonance, the higher the field strength.

III. STATE of the ART on the CURRENT EFFICIENCY of SOLAR CELLS

Today, there are various photovoltaic cell technologies characterized either by the materials used or by their very principle.

Firstly, there is the crystalline silicon-based sector, including mono and polycrystalline (first generation cells) which represents 88% of world production [7]. Then the thin-film sector (second generation cells) including amorphous silicon cells, multicrystalline or monocrystalline, cadmium tellurium, copper indium selenium, gallium

ISSN: 2356-5608

arsenide and organic materials. And finally the third generation cells in thin layers constituted by III-V semiconductor materials with single or multi-junction, nanocrystalline cells with dye (Gratzel cells) and perovskite cells.

According to a survey on the efficiency of solar cells, the highest efficiencies are obtained with III-V multi-junction cells under concentration while the lowest efficiencies are given by organic solar cells [8].

IV. COUPLING SOLAR CELL/RESONANT STACK

In this part, we will realize the coupling of these nanostructures exalting the optical field with a solar cell in order to expect record yields within the cell.

Thus, after having made a state of the art on the yields of different technologies of thin film photovoltaic solar cells, we were able to make an optimal choice on the model to be retained for the continuation of our work. This choice is based on its wide photonic gap going from 0.7 eV to 3.42 eV simply by changing the indium composition but also on its high absorption coefficient which is 10^5 cm^{-1} [9]. It is a solar cell structure based on Indium Gallium Nitride (InGaN) based on a Schottky contact, named "MIN structure" (Metal/InGaN-I/InGaN-N) with an efficiency of 19.8 % [10].

A. Description of the metal configuration

This configuration 1 is composed from top to bottom by:

- A superstrate (glass) that allows light penetration;
- A thin metallic layer of gold 50 nm thick;
- A thin metallic layer (platinum) of thickness 5nm to facilitate the penetration of photons;
- An intrinsic layer of 600nm thickness of InGaN lightly doped N where the Space Charge Zone (SCZ) will extend very largely because of its low concentration of dopants;
- A layer of InGaN doped with silicon which is commonly used and 830nm thick.
- And the whole is deposited on a substrate such as Sapphire with a buffer layer of Gallium Nitride (GaN) of thickness 503nm strongly doped N between the substrate and the cell.

The N-type ohmic metallizations are made on the surface of the highly doped GaN layer to ensure a good contact. The ohmic contacts on the front side are made in transverse with the Schottky contact. This configuration is shown in Fig. 5 below.

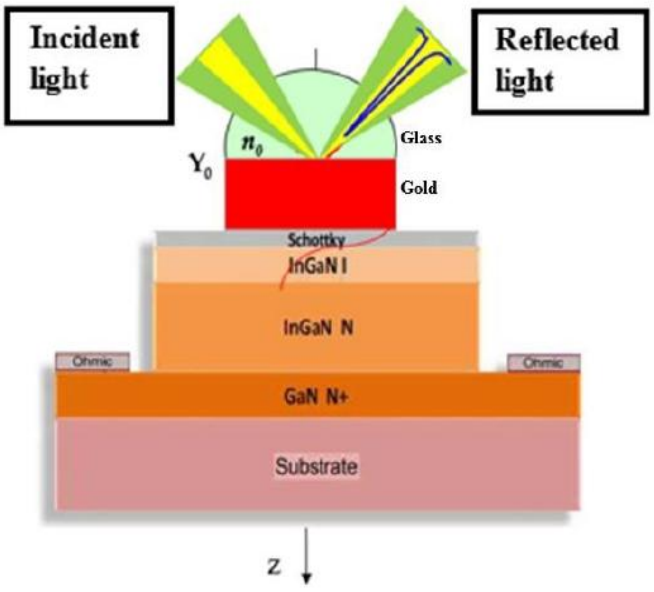

Fig. 5 Diagram of the metal configuration

B. Description of the multi-dielectric configuration

This configuration 2 is composed from top to bottom by:

- A superstrate (glass) that allows light penetration;
- An alternation of 4 thin dielectric layers of high and low index. The high index material used is Tantalum Pentaoxide (Ta_2O_5) and the low index material used is Silicon Dioxide (SiO_2).
- A thin metallic layer (platinum) 5nm thick to facilitate photon penetration;
- An intrinsic layer of 590nm thickness of InGaN lightly doped N where the Space Charge Zone (SCZ) will extend very largely because of its low concentration of dopants;

ISSN: 2356-5608

- A layer of InGaN doped with silicon which is commonly used and 830nm thick.
- And the whole is deposited on a substrate such as Sapphire with a buffer layer of Gallium Nitride (GaN) of thickness 410 nm strongly doped N between the substrate and the cell.

The N-type ohmic metallizations are made on the surface of the highly doped GaN layer to ensure a good contact. The ohmic contacts on the front side are made in transverse with the Schottky contact. This configuration is shown in Fig. 6 below.

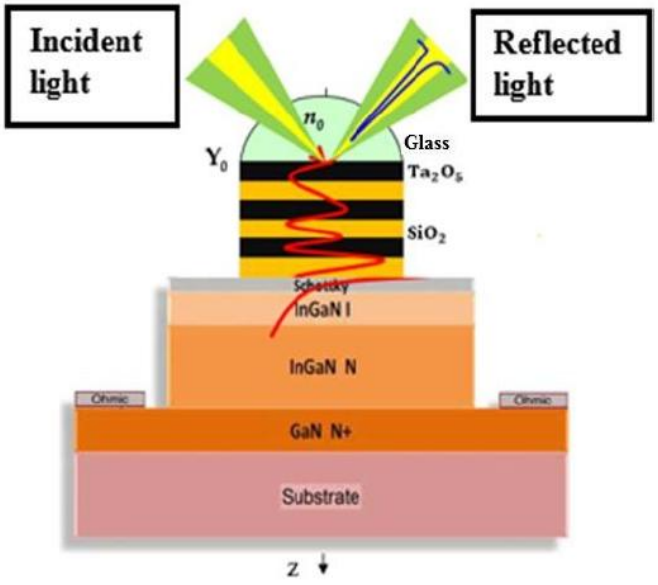

Fig. 6 Diagram of the multi-dielectric configuration

C. Final results of the coupling

In this part, we are mainly interested in the mapping of the absorption and field strength of its two configurations using Matlab/Simulink software.

1) *Results obtained by the metallic configuration:* The mapping of the absorption evolution as a function of wavelength and illumination angle corresponding to this configuration is calculated and presented in Fig. 7.

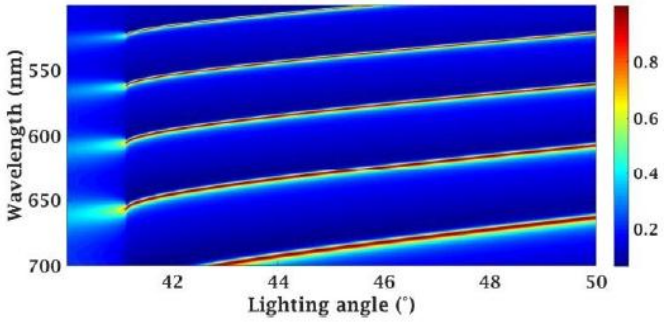

Fig. 7 Mapping of absorption as a function of wavelength and angle of incidence in TM mode with the metal configuration

In this figure, on all the areas a little reddish or even black; there are an infinite number of pairs of wavelength and angle of incidence where the absorption is maximum. In other words, many wavelengths are absorbed by the cell. Note also that this total absorption is often accompanied by an exaltation of the electric field. By representing the evolution of the latter for the metal configuration when the conditions of total absorption are met, we obtain the following Fig. 8.

ISSN: 2356-5608

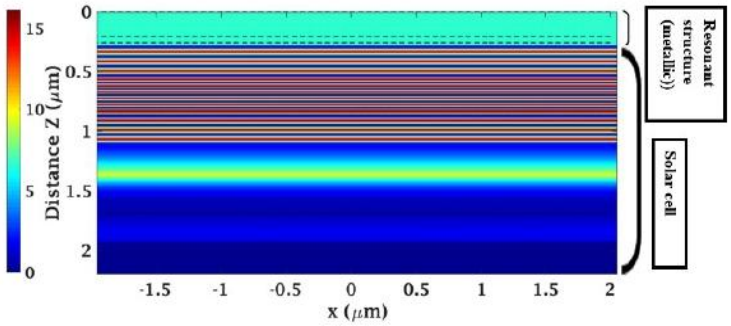

Fig. 8 Mapping of the electric field as a function of Z and X in TM mode when the metal configuration is illuminated at the resonance frequency

In this figure, on all the slightly reddish or even black lines, there are an infinite number of pairs of points of X and Z where the exaltation is maximum. In other words, the over intensification reaches a maximum value of 15 in the cell and this is due to the bandwidth of the resonance of the metal structure which is very wide.

2) *Results obtained by the multi-dielectric configuration:* The mapping of the absorption evolution as a function of wavelength and illumination angle corresponding to this configuration is calculated and presented in Fig. 9.

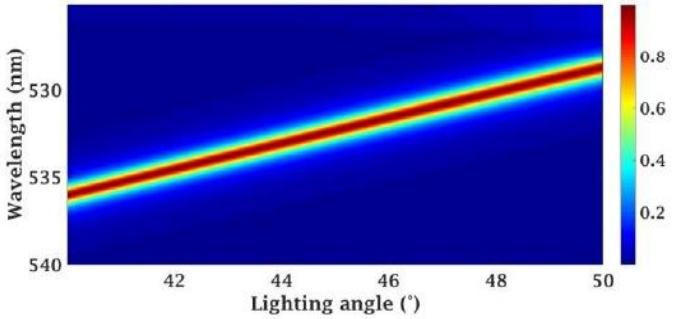

Fig. 9 Mapping of absorption as a function of wavelength and angle of incidence in TE mode with the multi-dielectric configuration. The materials used are Ta_2O_5 and SiO_2

Here, in the slightly reddish or even black area there are many pairs of wavelength and incidence from which the absorption is maximum. By representing the evolution of the associated electric field when the conditions of total absorption are met, we obtain Fig. 10 below.

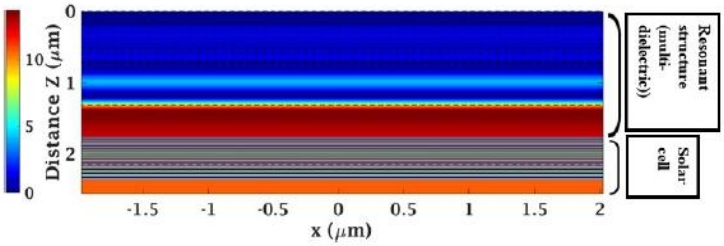

Fig. 10 Mapping of the electric field as a function of Z and X in TE mode when the multi-dielectric configuration is illuminated at the resonant frequency

In this figure, on all the slightly reddish or even black areas, there are an infinite number of pairs of points of X and Z where the exaltation is maximum. In other words the over intensification reaches a maximum value of 10 in the cell. This small value is a consequence of the fineness of the resonance. Indeed, the narrower the resonance, the fewer wavelengths are absorbed.

V. EVALUATION of EFFICIENCY

In this section, we will evaluate the yields obtained by the metallic configuration and the multi-dielectric configuration. To do so, we will first give the efficiency obtained by the control cell by simulation using Matlab/Simulink software.

Several loss factors are noted for the photovoltaic conversion within a solar cell. They often come from the nature of the material and the technology used for the realization of the latter.

For this, a solar cell exposed to solar radiation, can be modeled by the circuit of Fig. 11. It consists of a current source I_{ph} modeling the luminous flux in parallel with a diode that models the PN junction, a series resistance R_s representing the resistance related to the metal contacts, to the semiconductor layers and to the

ISSN: 2356-5608

metal/semiconductor interfaces whose value must be as small as possible to limit its influence on the cell current (in the ideal case, $R_s = 0$) and a shunt resistance R_{sh} which characterizes any leakage current caused by recombinations and defects in the structure which must be as high as possible (in the ideal case, $R_{sh} = \infty$) [11], [12]. The recombinations of the carriers in the space charge zone are translated by an ideality coefficient (A) which is an empirical factor that is equal to 1, for an ideal junction and takes a value between 1 and 2 when the recombination currents in the junction are considered.

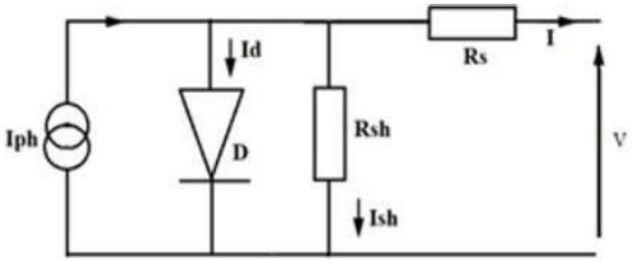

Fig. 11 Equivalent electrical diagram of the photovoltaic cell. R_S is the series resistance of the circuit. R_{Sh} is the parallel resistance of the circuit (shunt)

Other factors can also cause significant losses in the conversion efficiency of a photovoltaic cell. For example:

- Partial absorption of incident photons: incident photons of energy below the semiconductor gap ($h.\nu<E_g$) cannot generate electron-hole pairs and are therefore lost.
- Thermalization losses: an incident photon of energy greater than the gap ($h.\nu>E_g$) generates only one electron-hole pair; the excess energy is transferred as heat into the material.
- Losses due to the reflection of light radiation incident on the surface: only part of the solar radiation is absorbed, the other part being reflected.
- Losses due to the partial coverage of the cell surface by the metal contacts of the front panel.

From Fig. 11, the characteristic equation is deduced in a direct way from Kirchhoff's law.

$$I = I_{ph} - I_d - I_{sh} \qquad (1)$$

With:

I_{ph}: Photonic current.

I_d: Current through the diode.

I_{sh}: Current through the shunt resistor.

The diode being a non-linear element, its I-V characteristic is given by the relation:

$$I_d = I_o \left[\exp\left(\frac{q(V + I * R_s)}{n * A * K * T} \right) - 1 \right] \qquad (2)$$

and

$$I_{sh} = \frac{V + R_s * I}{R_{sh}} \qquad (3)$$

With

V: Voltage at the terminals of the diode.

n: Number of cells in series.

A: Factor of ideality of the junction or quality factor ($1<A<2$).

T: Operating temperature of the cell (K).

q: Electron charge constant ($1.602.10^{-23}$ C).

K: Boltzmann constant ($1.38.10^{-23}$ J/k).

R_{sh}: Shunt resistances representing leakage around the p-n junction due to impurities and cell corners.

R_s: Series resistance symbolizing the ground resistance of the semiconductor material, as well as the ohmic and contact resistances at the cell connections.

The saturation current of the diode I_0 is given by the following relation:

$$I_0 = I_{cc} \left(\frac{T}{T_{ref}} \right)^3 \exp\left[\frac{qE_g}{nK} \left(\frac{1}{T_{ref}} - \frac{1}{T} \right) \right] \qquad (4)$$

T_{ref}: Reference temperature of the cell (298K).

ISSN: 2356-5608

E_g: Energy of the Gap (1.84 eV for the InGaN to b=1.43 (curvature parameter) and x=0.45 (Indium composition)).

I_{cc}: Saturation current of the cell.

Photonic current related to illumination and temperature:

$$I_{ph} = [I_{cc} + Ki(T - T_{ref})] * \frac{G}{1000} \quad (5)$$

According to **Fig. 12**, the electric current produced by the cell is given by the following expression **[13]**.

$$I = I_{ph} - I_0 \left[\exp\left(\frac{q(V + I * R_s)}{n * A * K * T} \right) - 1 \right] - \frac{V + I * R_s}{R_{sh}} \quad (6)$$

After simulation with Matlab/Simulink software, we obtain the following **Fig. 12** and **Fig. 13** of the control cell.

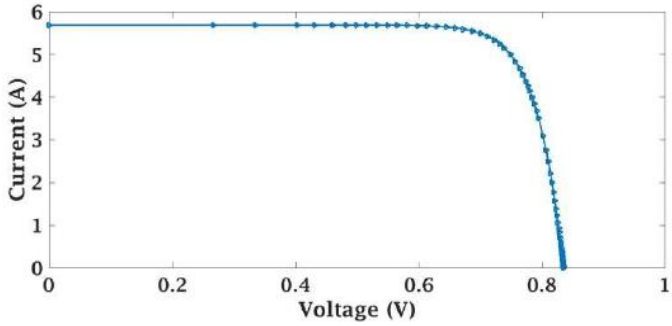

Fig. 12 Current-voltage characteristic I(V) of the control solar cell

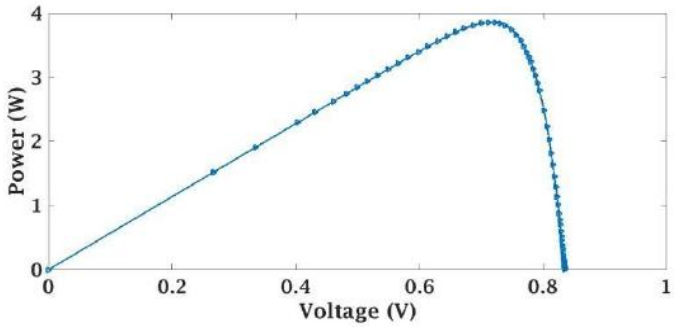

Fig. 13 Power-voltage characteristic P(V) of the control solar cell

The study of a photovoltaic cell uses five main characteristic quantities that derive from its current-voltage I(V) and power-voltage P(V) characteristics shown in Fig. 12 and Fig. 13, among which we can mention :

- The voltage of open circuit, noted V_{CO}=0.835V, maximum voltage at the terminals of the cell at zero current (I = 0), it depends mainly on the temperature of the cell and the spectrum of illumination.
- The short circuit current, I_{CC} = 5.69A, is the current flowing in the cell at zero voltage (V = 0), it depends mainly on the intensity of light and the surface of the cell.
- The filling factor (form factor), noted FF = 81.24%, is the ratio between maximum power supplied (P_m) on the product I_{CC} V_{CO}. It is always lower than 1
- The maximum power point, P_m=3.86W, obtained for an optimal current and voltage (I_m, V_m).
- The conversion efficiency (η=19.8%) of the control cell is defined by the ratio between the maximum power (P_m) and the power of the solar radiation incident (P_{inc}) on the photovoltaic cell:

$$\eta = \frac{P_m}{P_{inc}} = \frac{V_m * I_m}{P_{inc}} = \frac{FF * V_{co} * I_{cc}}{P_{inc}} = FF * V_{co} * J_{cc}$$

With

$$FF = \frac{V_m * I_m}{V_{co} * I_{cc}}$$

$$J_{cc} = \frac{I_{cc}}{P_{inc}}$$

J_{cc} : Current density.

ISSN: 2356-5608

$$I_{cc} = \frac{I_{ph}}{1 + \frac{R_s}{R_{sh}}}$$

$$V_{co} = \frac{K * T}{q} \ln\left(1 + \frac{I_{cc}}{I_o}\right)$$

A. Calculation of the efficiency for the metallic configuration

With this configuration, we could exalt the optical field by a factor of 10. Therefore, after simulation with Matlab/Simulink software, we obtained the following Fig. 14 and Fig. 15.

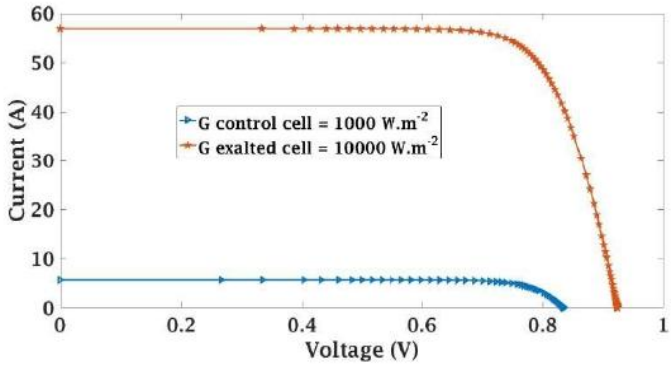

Fig. 14 Current-voltage characteristic of the solar cell coupled with the metallic configuration compared with the control solar cell

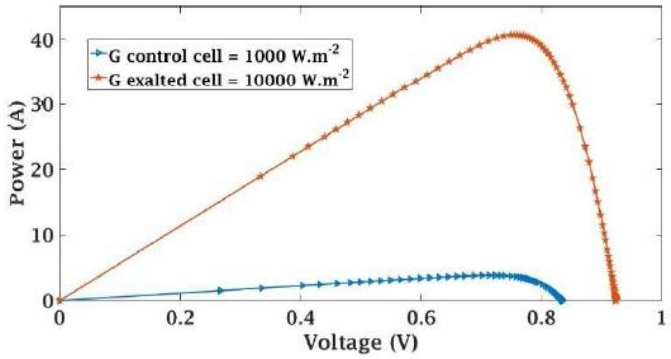

Fig. 15 Power-voltage characteristic of the solar cell coupled with the metallic configuration compared with the control solar cell

These figures represent the evolution of the current-voltage and power-voltage characteristics as a function of irradiation. We can easily see that it is the solar cell coupled with the metallic configuration which presents the best performances with an optimal output of 21.01% against 19.8% for the control solar cell. If we observe in a finer way these performances, we can notice that the solar cell coupled with the metallic configuration has the best I_{CC}=56.9A compared to 5.69A for the control cell and the best V_{CO}=0.9237V compared to 0.835V for the control cell but on the other hand a FF=77.57% which is lower than that of the control cell which is 81.24%. This is simply due to the coefficient of exaltation of the optical field before its arrival at the surface of the cell which is about 10.

B. Performance calculation for the multi-dielectric configuration

With this configuration, we have an amplification of the optical field by a factor of 14. Therefore, after simulation with Matlab/Simulink software, we obtain the following Fig. 16 and Fig. 17.

ISSN: 2356-5608

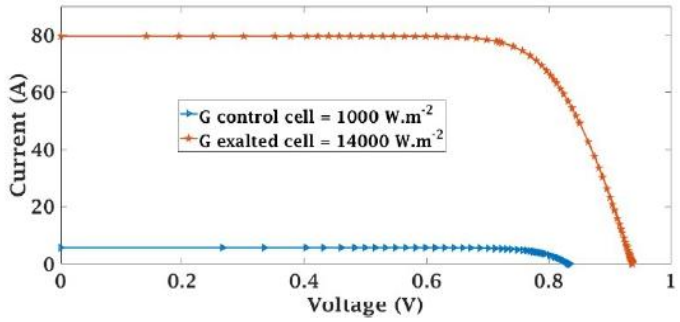

Fig. 16 Current-voltage characteristic of the solar cell coupled with the multi-dielectric configuration compared with the control solar cell

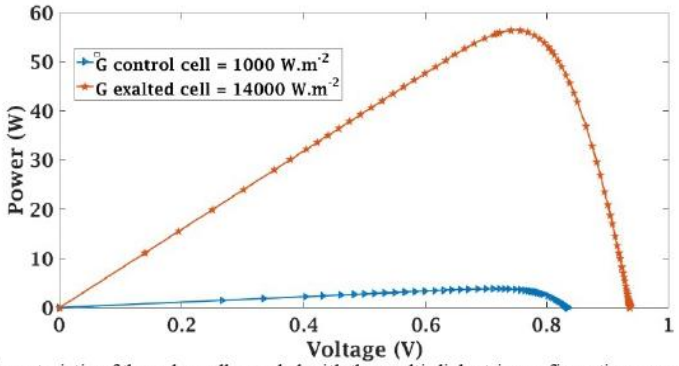

Fig. 17 Power-voltage characteristic of the solar cell coupled with the multi-dielectric configuration compared with the control solar cell

These two figures represent the current-voltage and power-voltage characteristics as a function of irradiation. Here also we can clearly see that it is the solar cell coupled with the multi-dielectric configuration which presents the best performances with an optimal output of 20.76% against 19.8% for the control solar cell. If we observe in a finer way these performances, we can notice that the solar cell coupled with the multi-dielectric configuration has the best I_{CC}=80A compared to 5.69A for the control cell and the best V_{CO}=0.9367V compared to 0.835V for the control cell but on the other hand a FF=75.24% which is lower than that of the control cell which is 81.24%. This is also due to the amplification coefficient of the optical field before its arrival at the surface of the cell which is about 14.

Now from the results obtained with these two configurations (metallic and multi-dielectric configuration), we will make a comparison of their performances. To do this, we could plot their current-voltage and power-voltage characteristics in Fig. 18 and Fig. 19.

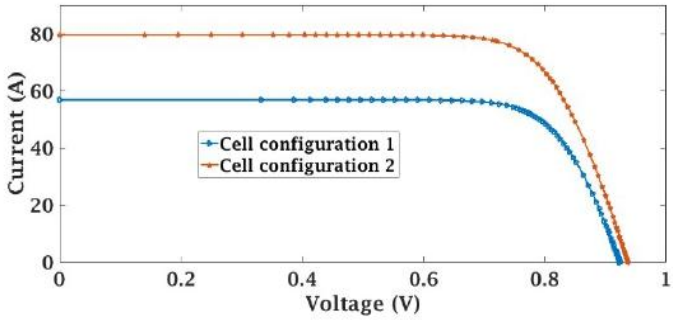

Fig. 18 Comparison of current-voltage characteristics of the two cell configurations

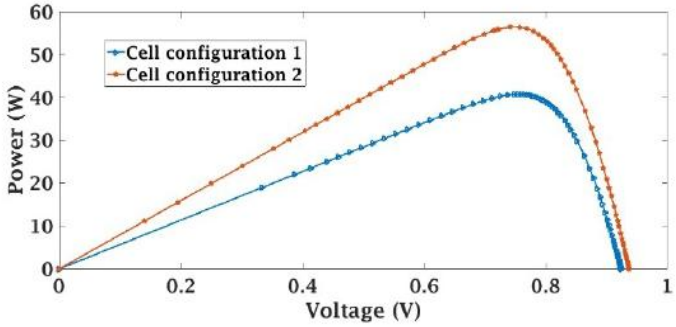

Fig. 19 Comparison of power-voltage characteristics of the two cell configurations

ISSN: 2356-5608

These figures represent the evolution of the current-voltage and power-voltage characteristics as a function of irradiation for the two cell configurations. From these two figures, we can see that the cell of configuration 2 has the best I_{CC}=80A compared to 56.9A for the cell of configuration 1 and the best V_{CO}=0.9367V compared to 0.9237V for the cell of configuration 1 but on the other hand a Form Factor FF=75.24% which is lower than that of the cell of configuration 1 which is 77.57%. Thus the efficiency obtained with the cell of configuration 1 is 21.01% against 20.76% for the cell of configuration 2.

Since the Form Factor (FF) indicates the effective surface of the material capable of transforming incident photons into electrons by photoelectric effect, this difference comes from the fact that the cell of configuration 1 has a very broad absorption band. In other words, several wavelengths can be absorbed over a more or less wide range of incidence. While the cell of configuration 2 has a much finer absorption band. In other words, few wavelengths can be absorbed over a more or less reduced range of incidence.

VI. CONCLUSION

In this paper, we have been able to plot the absorption and field maps for the metallic, multi-dielectric structure. We managed to couple these structures with the control cell while plotting with the help of Matlab/Simulink the maps of the absorption and the field for these two configurations. We could also evaluate the new yields obtained for each configuration which are 21.01% for the metallic configuration and 20.76% for the multi-dielectric configuration.

The new perspectives envisaged are the following:

- To study the effects of random and/or related errors of the thicknesses of the thin films during the deposition of the thin films on the absorption and on the field collected at the level of the absorbing layer;
- To study the scattering phenomena which are essentially due to the surface roughness during the deposition of thin films.

REFERENCES

[1] R. M. Goss, "BP statistical review of world energy 1982.," no. June, 2017.

[2] D. LINCOT, "La conversion photovoltaïque," *Découverte*, no. 344–345, pp. 47–65, 2007.

[3] C. Rodiet, M. Ramal, B. Rousseau, B. Garnier, and A. Djouadi, "Caractérisation thermique de couches minces par technique électrothermique : Validation numérique," in *SFT*, 2016, pp. 1–8.

[4] Yaël Thiaux, "Optimisation des profils de consommation pour minimiser les coûts économique et énergétique sur cycle de vie des systèmes photovoltaïques autonomes et hybrides Évaluation du potentiel de la technologie Li-ion," *Architecture*, p. 183, 2010.

[5] A. Adaine, S. Ould Saad Hamady, and N. Fressengeas, "Simulation study of a new InGaN p-layer free Schottky based solar cell," *Superlattices Microstruct.*, vol. 96, pp. 121–133, 2016.

[6] A. Sène, C. N. Ndiaye and L. Thiaw, "Absorption optimization in nano-structured optical thin films: Application to photovoltaic solar cells," *2022 IEEE International Conference on Electrical Sciences and Technologies in Maghreb (CISTEM)*, Tunis, Tunisia, 2022, pp. 1-6.

[7] "http://www.photovoltaique.info/Les-types-de-module.html.," Mars 2023.

[8] P. R. I. F. O. R. S. E. S. ISE, "Photovoltaics Report," no. May, 2022.

[9] A. Adaine *et al.*, "InGaN Metal-IN Solar Cell : optimized efficiency and fabrication tolerance To cite this version : HAL Id : hal-01523416," *China Fr. Second. Adv.*, 2017.

[10] M. A. Hoffbauer *et al.*, "device applications In-rich InGaN thin films : Progress on growth , compositional uniformity , and doping for device applications," vol. 114, no. May 2015, pp. 0–6, 2014.

[11] R. Algerienne, D. Et, M. D. E. L. Enseignement, S. D. E. La, F. D. E. Technologie, and D. D. E. G. Electrique, "Remerciement," 2022.

[12] I. H. Altas and A. M. Sharaf, "A photovoltaic array simulation model for matlab-simulink GUI environment," *2007 Int. Conf. Clean Electr. Power, ICCEP '07*, no. June, pp. 341–345, 2007.

[13] Y. Ducros, "Sciences et techniques," *Autres Temps. Les Cah. du Christ. Soc.*, vol. 31, no. 1, pp. 41–44, 1991.

ISSN: 2356-5608